Biochemical and Biophysical Research Communications **282,** 284–291 (2001)
doi:10.1006/bbrc.2001.4529, available online at http://www.idealibrary.com on IDEAL®

Asymmetric Arrangement of Auxiliary Subunits of Skeletal Muscle Voltage-Gated L-Type Ca^{2+} Channel

Kazuyoshi Murata,*[,1] Narumasa Odahara,* Akihiko Kuniyasu,† Yuhki Sato,† Hitoshi Nakayama,† and Kuniaki Nagayama*

**National Institute for Physiological Sciences, Myodaiji, Okazaki 444-8585, Japan; and †Department of Biofunctional Chemistry, Faculty of Pharmaceutical Sciences, Kumamoto University, 5-1 Ohe-honmachi, Kumamoto 862-0973, Japan*

Received February 16, 2001

Highly purified L-type Ca^{2+} channel complexes containing all five subunits (α_1, α_2, β, γ, and δ) and complexes of α_1-β subunits were obtained from skeletal muscle triad membranes by three-step purification and by 1% Triton X-100 treatment, respectively. Their structures and the subunit arrangements were analyzed by electron microscopy. Projection images of negatively stained Ca^{2+} channels and α_1-β complexes were aligned, classified and averaged. The α_1-β complex showed a hollow trapezoid shape of 12 nm height. In top view, four asymmetric domains surrounded a central depression predicted to form the channel pore. The complete Ca^{2+} channel complex exhibited the cylindrical shape of 20 nm in height binding a spherical domain on one edge. Further image analysis of higher complexes of the Ca^{2+} channel using a monoclonal antibody against the β subunit showed that the α_1-β complex forms the non-decorated side of the cylinder, which can traverse the membrane from outside the cell to the cytoplasm. Based on these results, we propose that the Ca^{2+} channel exhibits an asymmetric arrangement of auxiliary subunits.

Key Words: **voltage-gated Ca^{2+} channels; subunit arrangement; skeletal muscle; single particle analysis; electron microscopy; protein structure.**

The skeletal muscle voltage-gated L-type Ca^{2+} channel is a heteromeric complex consisting of five distinct subunits (α_1, α_2, β, γ and δ) (1). The α_1 subunit is a transmembrane protein of 175 kDa with four homologous domains (or repeats), each of which contains six predicted membrane-spanning segments (2). The α_1 subunit can serve as a principal functional component of the voltage sensor and ion pore. The domain structure of the α_1 subunit is similar to that of both Na^+ and K^+ channel α subunits (3). As regulatory modules, four auxiliary subunits are associated with α_1 subunit. The β subunit is a protein of 55 kDa, which is uniformly hydrophilic and non-glycosylated and is thought to be intracellular (4). The α_2 subunit of 143 kDa and the δ subunit of 25-17 kDa, both of which are heavily glycosylated, are derived from a single protein precursor and linked by a disulfide bond after proteolysis (5, 6). The δ subunit, a single transmembrane segment, has three forms (δ_1, δ_2 and δ_3) generated by different proteolytic processing (7). They anchor the α_2 subunit, which is possibly located extracellularly (8–10). The γ subunit of 30 kDa, a glycoprotein containing predicted transmembrane segments, is found only in skeletal muscle Ca^{2+} channels (11). Functional analysis of individual auxiliary subunits has been undertaken with electrophysiological methods using exclusive or heterologous expression systems in *Xenopus* oocytes and mammalian cell lines (12–18).

In contrast to functional electrophysiological and pharmacological investigations (19, 20), structural knowledge about voltage-gated Ca^{2+} channels at three-dimensional (3D) level has not been available primarily due to the difficulty in obtaining sufficient quantities of pure proteins to undertake 3D crystallization and to make large well-ordered 3D crystals required for high-resolution X-ray crystallographic analysis. Nevertheless, some predicted structural models have been proposed (21, 22).

Recently atomic models of two bacterial ion channels, *Saccharomyces lividens* K^+ channel (23) and *Mycobacterium tuberculosis* mechanosensitive ion channel (24), have successively been determined by X-ray crystallography. While these channels are not voltage-gated ion channels, the mechanisms of ion selective filtration and the pore gating, which universally equipped with voltage-gated ion selective channel, are described using the atomic models. As the first charac-

Abbreviations used: 2D, two-dimensional; 3D, three-dimensional; DTT, dithiothreitol; EDTA, ethylenediamine tetraacetic acid; PAGE, polyacrylamide gel electrophoresis; SDS, sodium dedecylsulfate; WGA-Sepharose, wheat germ agglutinin-Sepharose.

[1] To whom correspondence should be addressed. Fax: +81-564(52)7913. E-mail: kazum@nips.ac.jp.

0006-291X/01 $35.00

terized channel protein from higher organism, the human water channel (aquaporin1), has been determined at 3.8 Å resolution by electron crystallography using two-dimensional (2D) crystals (25). These models of non-ion channels revealed that the selectivity in the pore is also achieved with the pore helices similar to that of the K^+ channel. On the other hand, structural studies of voltage-gated ion channels have been restricted to low-resolution structures. Very recently, detergent-solubilized structure of electric eel Na^+ channel was analyzed by single particle analysis of cryo-electron microscopy at 19 Å resolution (26). The described bell shape of the Na^+ channel has the appearance of a four-fold symmetric tetramer deduced from the four repeats sequence, with a large, central vestibule that presumably constitutes part of the pathway for ions.

Protein crystallization is required to achieve higher resolution in 3D structural analysis, even in electron microscopy. So far, some 3D and 2D protein crystals of membrane proteins have been produced and analyzed after overcoming various technical difficulties. In many cases, proteins are modified to make them more suitable for crystallization using deletion or mutation techniques. Single particle analysis of proteins by electron microscopy, although of low resolution, is of value because no such modification of proteins occurs.

Here, we report single particle images of the skeletal muscle voltage-gated Ca^{2+} channel and its α_1-β complex at about 30 Å resolution by electron microscopy. The Ca^{2+} channel with all five subunits and an α_1-β complex were isolated for single particle analysis. Negatively stained molecular images, each of which displays a different projection, were classified and averaged by multivariate statistical analysis, and the three-dimensional structure of the complexes was deduced from some class-averaged projections. Further image analysis of the Ca^{2+} channel complex using a monoclonal antibody against the β subunit indicated the topological orientation of the Ca^{2+} channel in the cell membrane and the localization of the auxiliary subunits. From analysis of these projections, we propose the asymmetric localization of auxiliary subunits surrounding the central α_1 subunit.

MATERIALS AND METHODS

Isolation and purification of Ca^{2+} channel complexes. Triad membranes were isolated from rabbit skeletal muscle as described (27). The following isolation and purification of Ca^{2+} channel complexes was carried out with a three-step purification procedure, which is a modification of the protocol of Kuniyasu *et al.* (28). Extract of triad membranes treated with 1%-digitonin in 20 mM Tris-HCl (pH 7.4) containing 0.5 M NaCl were first loaded onto a WGA-Sepharose column after radiolabeling with a dihydropyridine calcium antagonist [^{3}H] PN200-100 (NEN Inc.). Protein fractions binding [^{3}H] PN200-100 were eluted with 6% N-acetylglucosamine (GlcNAc). Then, GlcNAc pools were layered onto a linear gradient of 5-20% (w/w) sucrose and fractionated by sucrose density gradient sedimentation at 27,000 rpm on a Beckman SW28 rotor for 13 h. Radioactive fractions were further loaded onto a heparin-agarose column and eluted with a linear gradient of 0.1–0.5 M NaCl in 20 mM Tris-HCl (pH 7.4) containing 0.3% CHAPS and 0.1 mM $CaCl_2$ (buffer A). Purified skeletal muscle Ca^{2+} channels were stored at −80°C. The α_1-β complex was further isolated from the purified channels by a modification of methods described by Takahashi *et al.* (1). The purified Ca^{2+} channels were treated with 1% (w/v) Triton X-100 for 2 h at 4°C and loaded onto a WGA-Sepharose column to remove α_2-δ complexes and Ca^{2+} channels consisting of all subunits. Furthermore, the α_1-β complex that passed through a WGA-Sepharose column was fractionated on a heparin-agarose column, in which γ subunit was passed through the column. After washing the column two times with buffer A plus 0.1 M NaCl, the α_1-β complex was eluted with 0.5 M NaCl as described above. Purified samples were analyzed on 5–15% SDS-PAGE gels (29) and a sample buffer containing 10 mM Tris-HCl (pH 7.6), 1% (w/v) SDS, 4 mM EDTA and 2% (w/v) sucrose. Samples were treated with and without reducing agents (20 mM DTT) at 60°C for 30 min. After SDS-PAGE, the gels were stained by Coomassie Brilliant Blue (CBB).

Electron microscopy. The isolated Ca^{2+} channel and α_1-β complex were subjected to gel-filtration chromatography to remove some contaminants and degradation products before specimen preparing for electron microscopy. The purified protein complexes (50 μl) were injected on a Superdex 200PC 3.2/30 column mounted in a Smart system (Pharmacia Biotech Inc.) and eluted with the sample buffer. The eluted protein peak fraction (3 μl) monitored at 280 nm was applied to a carbon-coated copper grid pre-treated by glow discharging, and stained with a 2 (w/v) % uranyl acetate solution after removing extra sample solution. The grids were then blotted with filter paper and dried in air. The sample grids were placed in a transmission electron microscope JEM1200EX (JEOL Inc.) working at an accelerating voltage of 100 kV. Electron micrographs were recorded with under focuses of 300-600 nm at a magnification of 25,000 on SO163 electron image films (Kodak Inc.) and developed with D19 developer (Kodak Inc.) for 12 min.

Image processing. Micrographs were checked not to contain serious astigmatisms with an optical diffractometer and then digitized with a pixel size of 5.6 Å at specimen level using a PHODIS film scanner (Zeiss Inc.). The following image processing was done with the SPIDER & WEB software (30) on an IRIX operating system (Silicon Graphics Inc.). Each particle image of the Ca^{2+} channel complex was cut out at 80 × 80 pixel frame from micrographs using the automated particle selection procedure based on discrimination function, while that of α_1-β complex was done at 40 × 40 pixel frame. Extraneous images and particles that are out of frames were interactively removed from the data set. The alignment and averaging of particles were performed according to multi-reference alignment and classification procedures (31). This refinement step was iterated until no further migrations of images between classes occur, and the class average images were generated. Furthermore, this alignment procedure was repeated using the newly selected data set in which 20% of poorly correlated images are removed. The dominant average images in the data set were then estimated. The original data set was again classified and aligned for the dominant particle images, and the resolution of the cluster-averaged images were assessed with the Fourier ring correlation method (32, 33). The averaged particle images were finally determined by removing poorly correlated data until the resolution did not improve.

Antibody labeling of the Ca^{2+} channel. A monoclonal antibody against β subunit of the skeletal muscle Ca^{2+} channel (clone VD2-1B12, Upstate Biotechnology, Lake Placid, NY) was used for the partial labeling of the Ca^{2+} channel. An excess antibody was added to the purified Ca^{2+} channel, and incubated for 4 h at 4°C. Free antibodies were removed by gel-filtration chromatography as mentioned above. The peak fraction was directly applied to a carbon-coated grid and negatively stained complex images were recorded, digitized and cut out as described above.

TABLE 1

Purification of the Skeletal Muscle Ca^{2+} Channel

Purification step	Receptor (pmol)	(%)	Protein (mg)	Specific activity (pmol/mg)	Purification (fold)
Triad membrane	8,970	100	390.0	23.0	1
WGA-Sepharose	5,188	57.8	9.24	261.5	11.4
Sucrose gradient centrifugation	1,827	20.4	4.2	435.0	18.9
Heparin-agarose	1,023	11.4	1.65	620.9	27.0

RESULTS AND DISCUSSION

Isolation and purification of skeletal muscle Ca^{2+} channel complexes. The skeletal muscle Ca^{2+} channel was isolated and purified from triad membranes by a three step purification, a protocol similar the four step procedure described by Curtis and Catterall (34) (Table 1). Specific binding activity of the purified Ca^{2+} channel to dihydropyridine [^{3}H]PN200-110 was 620.9 pmol/mg of protein. This value was much lower (27%) than the theoretical maximal specific activity of 2,325 pmol/mg of protein, based on 430 kDa as the molecular mass of the Ca^{2+} channel containing all five subunits. However, it has been reported that considerable amounts (27–53%) of dihydropyridine ligand dissociate from the Ca^{2+} channel-dihydropyridine ligand complex at every step during purification (34), suggesting that our observed specific activity is likely an underestimate. The purity of the Ca^{2+} channel obtained after heparin-agarose chromatography was also investigated by SDS-PAGE followed by CBB staining (Fig. 1). The purified Ca^{2+} channel showed four polypeptides identified as α_2-δ (175 kDa), α_1 (170 kDa), β (55 kDa), and γ (30 kDa) when analyzed on a 5–15% polyacrylamide gel under non-reducing conditions (lane 1). Densitometric scans revealed that stoichiometric ratio of the four polypeptides was 1.00:0.98:1.10:0.97, which compromised 95.1 $\pm$ 0.6% (average of three runs) of the CBB-stained intensity in the gel lane. Under reducing conditions (with DTT), the molecular weight of the 175 kDa polypeptide shifted to 150 kDa (α_2) due to removal of the disulfide-bonded δ subunit (lane 2) indicating that the purified Ca^{2+} channel contained six polypeptides of α_1 (170 kDa), α_2 (150 kDa), β (55 kDa), γ (30 kDa), and δ_1 (27 kDa)/δ_2 (23 kDa). Densitometric quantification revealed that ratio of the six polypeptides was 1.00:1.06:1.00:1.14:0.21:0.47, which explained 95% of the CBB-stained intensity. Although the extensive study focused on δ subunits is reported (7) to observe three δ subunits (δ_1, δ_2, and δ_3), only two (δ_1 and δ_2) of them were apparently observed on the 5-15% gradient polyacrylamide gel used in this work.

An $\alpha_1-\beta$ complex was obtained after treating purified Ca^{2+} channels with 1% Triton X-100, followed by heparin-agarose column chromatography. The composition of the α_1-β complex was confirmed by SDS-PAGE, which indicated the presence of only two polypeptides of α_1 (170 kDa) and β (55 kDa) (stoichiometric ratio = 1.00:1.02), whose mobility did not change after reduction (Fig. 1, lanes 3 and 4). Treatment with 1% Triton-X 100 resulted in considerable loss of [^{3}H]PN200-110 binding activity (data not shown). From 1.65 mg of purified Ca^{2+} channel, we obtained 0.25 mg of α_1-β complex, which corresponds to a 15% yield.

Solubilized Ca^{2+} channels are stabilized by addition of phospholipids after elution from heparin-agarose columns. However, these phospholipids greatly increased background noise in electron microscopy and were omitted in this study. We employed gel-filtration chromatography immediately before the sample was subjected to electron microscopy and obtain the highly dispersed single particles of Ca^{2+} channel on carbon support film, which gives low background noise (Fig. 2).

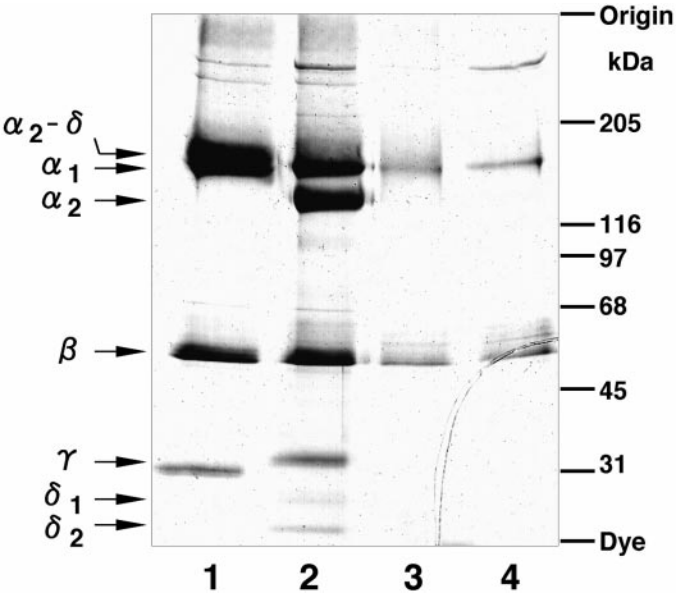

FIG. 1. Subunit composition of the purified skeletal muscle Ca^{2+} channel and α_1-β complex. The purified Ca^{2+} channel (lanes 1 and 2) and α_1-β complex (lanes 3 and 4), which were treated with (reducing conditions, lanes 2 and 4) or without 20 mM DTT (nonreducing conditions, lanes 1 and 3), were separated by SDS-PAGE using a 5–15% gradient gel and stained with CBB.

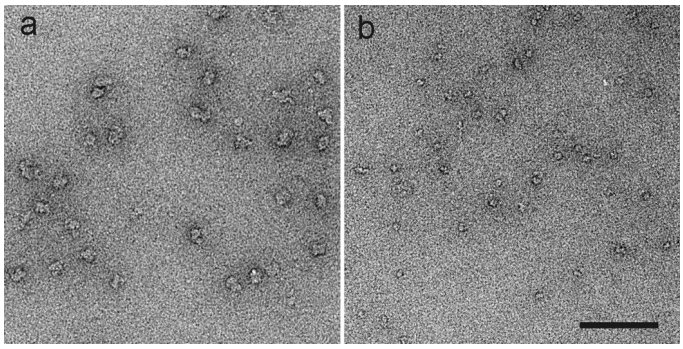

FIG. 2. Negatively stained images of purified skeletal muscle Ca^{2+} channel complexes and α_1-β complexes: (a) Ca^{2+} channel complexes, (b) α_1-β complexes. Samples were stained with 2% uranyl acetate on the carbon support film and imaged on an electron microscope. Scale bar indicates 50 nm.

Visualization and image processing of Ca^{2+} channel complexes. Single particles of the purified Ca^{2+} channel and α_1-β complex were stained with 2% uranyl acetate on carbon support film, and the projections were recorded on electron films at an appropriate magnification (Fig. 2). For the α_1-β complex image processing, 1571 images were selected from three micrographs and subjected to the multi-reference alignment, in which 20 classes were defined and the refinement step was iterated 15 times. The resultant cluster-averaged images also contained similar shape images or poorly correlated blurred images. Therefore, such multi-reference alignment was further iterated at conditions that gradually removed low correlation images and reduced the number of clusters. Finally four kinds of dominant projections in the α_1-β complex were estimated from 119 selected images. The original data set was again classified and aligned for such reference images, and after removing low correlation images, four final projections of the α_1-β complex were calculated from 776 selected images, which show the highest resolution value (Fig. 3). The number of averaged images in each projection were 157, 197, 131, and 291 as indicated in Figs. 3a–3d, respectively, and their reso-

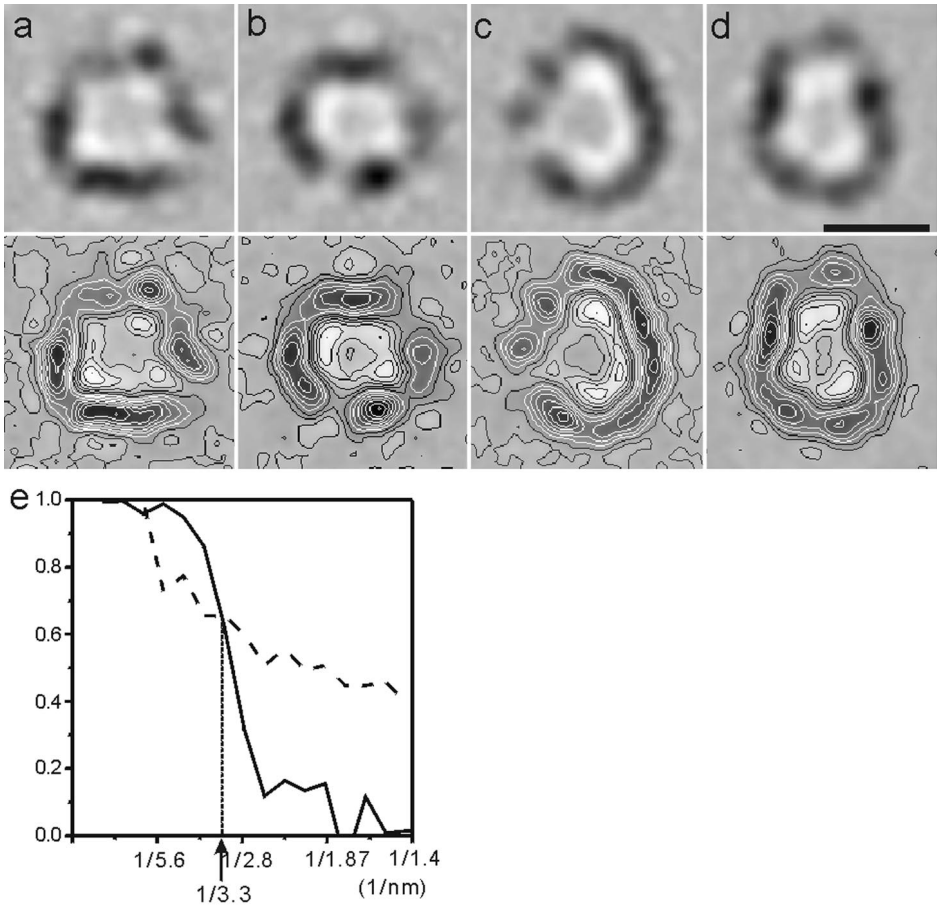

FIG. 3. Image analysis of the solubilized α_1-β complex. Four cluster averaged projections calculated by multivariate statistical analysis are displayed without contours (top) and with contours (bottom), which exhibit two square shape (a, b) and two trapezoid shape (c, d). Scale bar indicates 10 nm. (e) The representative Fourier ring correlation function (solid line) calculated from the data set of panel a and its critical ring correlation function (3σ; dashed line). The attainable resolution of the image was decided from the cross point of two correlation curves.

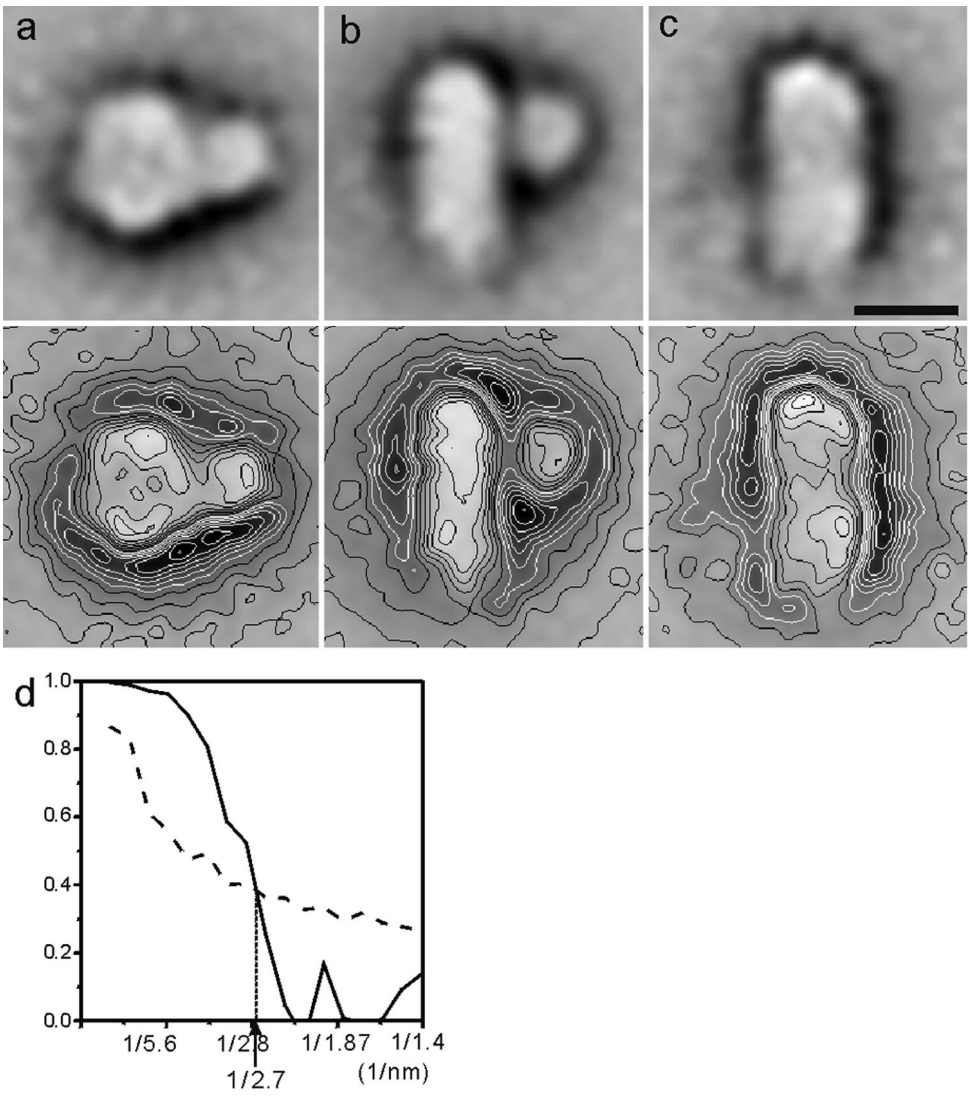

FIG. 4. Image analysis of the solubilized Ca^{2+} channel complex. Three cluster averaged projections are displayed without contours (top) and with contours (bottom), which are interpreted as one top view (a) and two side views (b, c). Scale bar indicates 10 nm. (d) The representative Fourier ring correlation function (solid line) calculated from the data set of b and its critical ring correlation function (3σ; dashed line). The attainable resolution of the image was decided from the cross point of two correlation curves.

lutions estimated from Fourier ring correlation were 3.3, 3.4, 3.5, and 3.5 nm, respectively.

Images of Ca^{2+} channel were also detected from four micrograms that have no astigmatism, and 2613 particles were interactively selected. The selected particle images were subjected to the multi-reference alignment, 30 classes were defined, and a series of the processing was iterated 15 times. Three kinds of dominant projections of Ca^{2+} channel were then estimated using the same procedure followed for the α_1-β complex. Finally, three cluster-averaged images of the Ca^{2+} channel showing the best resolution values were generated from 1945 image sets after removal of low correlation images (Fig. 4). The numbers of averaged images in each projection were 746, 506 and 693 from Figs. 4a to 4c, respectively, and the resultant resolutions were estimated at 3.0, 2.7, and 2.8 nm, respectively.

Structure of the α_1-β complex. Projections of the α_1-β complex exhibited two square shapes (Figs. 3a and 3b) and two trapezoid shapes (Figs. 3c and 3d) that are quite similar to that of the electric eel Na^+ channel (26, 35). Therefore, we referred to top views (Figs. 3a and 3b) and side views (Figs. 3c and 3d) according to notations used in describing the Na^+ channel. In top views, two types of square appeared as a large end 10 nm wide (Fig. 3a) and a smaller end 9 nm wide (Fig. 3b). The squares were constructed with four repeated domains of the α_1 subunit with a central vestibule 2nm in width that presumably constitutes the ion pathway. Furthermore, the large square end exhibited asymmetric do-

mains, while the small square end was more symmetric. Although Sato *et al.* also reported that the Na^+ channel is constructed from four different-sized domains (35), the α_1-β complex of the Ca^{2+} channel exhibits domains that are more asymmetric than the Na^+ channel, one of which protrudes beyond the square. Despite its sequence similarity with the α subunit of the Na^+ channel, the remarkable asymmetry of the Ca^{2+} channel is presumably due to the β subunit, which interacts with the cytoplasmic I-II loops of the α_1 subunit (5). The α_1 subunit of skeletal muscle voltage-gated Ca^{2+} channel also interacts with ryanodine receptors in the sarcoplasmic reticulum through both cytoplasmic loops II-III and the C-terminal domain of the α_1 subunit (36, 37). It is unclear whether the interaction is direct or via the junction protein, triadin, also proposed to interact directly with loops II-III (38). Furthermore, both the α_1 subunit and the cytoplasmic β subunit are substrates for protein kinases *in vitro,* and phosphorylation of these subunits may regulate the function of the channel *in vivo* (3, 39–41). These observations suggest that the cytoplasmic surface of the α_1 subunit is not completely covered by the intracellular β subunit, and that the α_1 subunit is directly exposed to cytoplasm in some parts. Thus, the β subunit, which unlike the α_1 subunit has no repeating sequences, may localize on the fourfold symmetric domains of the α_1 subunit in an asymmetric manner with a stoichiometry of 1:1. The small square end of the top views also shows slight asymmetry (Fig. 3b), which may be due to the fact that the α_1 subunit undergoes a conformational change by binding to the β subunit (42, 43). The two side views were seen as a trapezoid shape 12 nm high (Figs. 3c and 3d), and the sizes of the top and bottom sides in these side views possibly coincide with the sizes of the two square top views, respectively (Figs. 3a and 3b). The side views also had a dark central region 2 nm wide, suggesting the location of the stain-filled cavity seen in the two top views. From these independent projections, the α_1-β complex was assumed to exhibit an inverted green pepper-like shape 12 nm high and 9-10 nm wide, having a central hole passing along the quasi-fourfold symmetrical axis. Furthermore, the cytoplasmic long loops between the four domains of the α_1 subunit and the existence of a cytoplasmic β subunit suggest that the open edge constituted from the asymmetric large square is orientated to the cytoplasm and the closed edge of the more symmetrical small square is oriented extracellularly.

Structure of the Ca^{2+} channel and the localization of auxiliary subunits. Three dominant projections generated from negatively stained Ca^{2+} channel complexes were interpreted as one top view (Fig. 4a) and two side views (Figs. 4b and 4c) from a comparison with that of the α_1-β complex. The two side views exhibited a rod shape 20 nm high and 9 nm wide, and the rod seen in

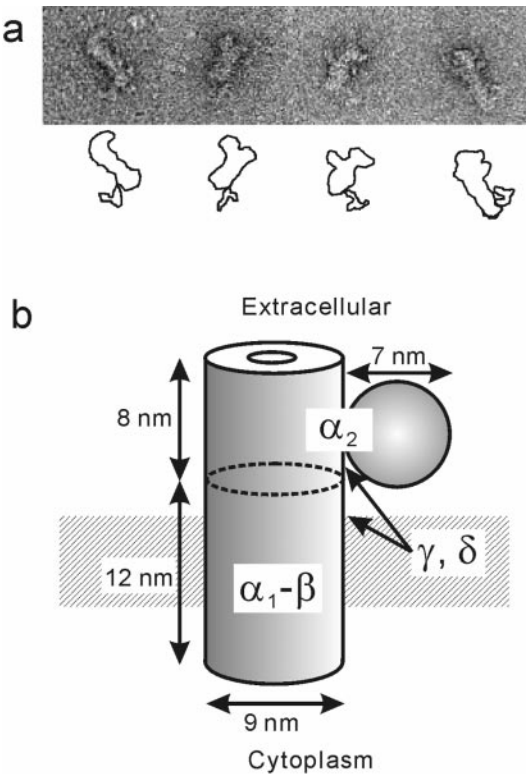

FIG. 5. (a) Negatively stained images of the complex, the Ca^{2+} channel and the anti-β subunit monoclonal antibody. The contours of the molecules of the Ca^{2+} channel and the antibody were indicated below. (b) A simplified structural model of the Ca^{2+} channel complex. The expected positions of each subunit in Ca^{2+} channel complex are indicated. A stripe band indicates the expected cell membrane position.

one side view bound a 7 nm spherical domain on one edge (Fig. 4b). Thus, two side views could be interpreted as the same one displayed at the different angles. On the top view, the rod seen in the side view resembles a quasi-pentagon accommodating the 7nm spherical domain on one side. In the center of the pentagonal main body, some unstained patches were identified, while a center-vestibule surrounded by four domains was filled with a stain in the α_1-β complex. In addition, the fact that there are no dark central regions in the rod part seen in side views suggests that the entrance to the ion passage is highly restricted by auxiliary subunits in the solubilized Ca^{2+} channel complex.

The Ca^{2+} channel complex has a large and highly-glycosylated α_2 subunit, which is most likely to be localized extracellularly and anchored to the integral α_1 subunit through the membrane spanning δ subunit. The generated projections of the Ca^{2+} channel complex were 8 nm longer than that of the α_1-β complex, and the spherical domain further decorated one edge of the main rod. Based on the shape and size of the α_1-β complex described in the previous section, the α_1-β complex could be assigned to the main rod. The puri-

fied Ca^{2+} channel was incubated with a monoclonal antibody against the β subunit and negatively stained images were observed. This antibody binds to the edge of the non-decorated rod part of the Ca^{2+} channel to form the complex (Fig. 5a), suggesting that the non-decorated part of the main rod is the α_1-β complex 12 nm high, which forms the transmembrane and cytoplasmic region of the Ca^{2+} channel. Therefore, the other region 8 nm high containing a spherical domain is assigned to the extracellular α_2 subunit. To summarize, we simplified the structure of the Ca^{2+} channel complex to a cylinder, 9 nm wide and 20 nm high, decorated with a 7 nm ball on one edge as shown in Fig. 5b. By assumption, the volume of α_1-β complex, which has a molecular weight of 230 kDa (= 175 kDa + 55 kDa), is calculated to be 763 nm^3. Assuming that protein density is constant throughout the Ca^{2+} channel complex, the molecular weight of the non α_1-β complex area, whose volume is 688 nm^3, is estimated to be 207.5 kDa. Although the calculated molecular weight is greater than that of α_2 subunit polypeptide, 143 kDa, it would be plausible if the α_2 subunit is considered as highly glycosylated, as are δ and γ subunits. Consequently, the α_2 subunit could be allocated to the area of the 7 nm ball and the ball-decorated cylinder 8 nm high, which is oriented extracellularly, while the α_1-β complex is assigned to the non-decorated cylinder 12 nm high, which is oriented to the membrane and cytoplasm. The membrane integral δ and γ subunits are probably included in the main cylinder.

Here for the first time, we describe the three-dimensional structure of the skeletal muscle voltage-gated L-type Ca^{2+} channel complex, based on cluster-averaged projections generated by multivariate statistical analysis of negatively stained images. Moreover, by antibody-labeling and comparison of the structures of both the Ca^{2+} channel and α_1-β complexes, the positions of the α_2 and β subunits relative to the central α_1 subunit were deduced, which consequently indicates the topology of the asymmetric Ca^{2+} channel complex across the plasma membrane. It is unclear why the auxiliary subunits are arranged around the channel forming α_1 subunit so asymmetrically, but the voltage-gated Ca^{2+} channel from skeletal muscles is known to functionally interact with the asymmetric foot of the ryanodine receptor in the sarcoplasmic reticulum (44). The unique asymmetric feature of the Ca^{2+} channel complex must be further confirmed by more detailed structural analyses in the future.

ACKNOWLEDGMENTS

We thank Miss Aiko Furukawa for her excellent technical assistance. This work was supported by a Grant-in-Aid for Scientific Research (12470483) from the Ministry of Education, Science, Sports and Culture of Japan and a grant from CREST (Core Research for Evolutionary Science and Technology) of Japan Science and Technology Corporation (JST) to H.N.

REFERENCES

1. Takahashi, M., Seagar, M. J., Jones, J. F., Reber, B. F., and Catterall, W. A. (1987) *Proc. Natl. Acad. Sci. USA* **84,** 5478–5482.
2. Tanabe, T., Takeshima, H., Mikami, A., Flockerzi, V., Takahashi, H., Kangawa, K., Kojima, M., Matsuo, H., Hirose, T., and Numa, S. (1987) *Nature* **328,** 313–318.
3. Catterall, W. A. (1988) *Science* **242,** 50–61.
4. Ruth, P., Rohrkasten, A., Biel, M., Bosse, E., Regulla, S., Meyer, H. E., Flockerzi, V., and Hofmann, F. (1989) *Science* **245,** 1115–1118.
5. Ellis, S. B., Williams, M. E., Ways, N. R., Brenner, R., Sharp, A. H., Leung, A. T., Campbell, K. P., McKenna, E., Koch, W. J., and Hui, A. (1988) *Science* **241,** 1661–1664.
6. De Jongh, K. S., Warner, C., and Catterall, W. A. (1990) *J. Biol. Chem.* **265,** 14738–14741.
7. Jay, S. D., Sharp, A. H., Kahl, S. D., Vedvick, T. S., Harpold, M. M., and Campbell, K. P. (1991) *J. Biol. Chem.* **266,** 3287–3293.
8. Brickley, K., Campbell, V., Berrow, N., Leach, R., Norman, R. I., Wray, D., Dolphin, A. C., and Baldwin, S. A. (1995) *FEBS Lett.* **364,** 129–133.
9. Gurnett, C. A., De Waard, M., and Campbell, K. P. (1996) *Neuron* **16,** 431–440.
10. Wiser, O., Trus, M., Tobi, D., Halevi, S., Giladi, E., and Atlas, D. (1996) *FEBS Lett.* **379,** 15–20.
11. Jay, S. D., Ellis, S. B., McCue, A. F., Williams, M. E., Vedvick, T. S., Harpold, M. M., and Campbell, K. P. (1990) *Science* **248,** 490–492.
12. Hofmann, F., Biel, M., and Flockerzi, V. (1994) *Annu. Rev. Neurosci.* **17,** 399–418.
13. Perez-Reyes, E., Kim, H. S., Lacerda, A. E., Horne, W., Wei, X. Y., Rampe, D., Campbell, K. P., Brown, A. M., and Birnbaumer, L. (1989) *Nature* **340,** 233–236.
14. Lacerda, A. E., Kim, H. S., Ruth, P., Perez-Reyes, E., Flockerzi, V., Hofmann, F., Birnbaumer, L., and Brown, A. M. (1991) *Nature* **352,** 527–530.
15. Varadi, G., Lory, P., Schultz, D., Varadi, M., and Schwartz, A. (1991) *Nature* **352,** 159–162.
16. Ren, D., and Hall, L. M. (1997) *J. Biol. Chem.* **272,** 22393–22396.
17. Mikami, A., Imoto, K., Tanabe, T., Niidome, T., Mori, Y., Takeshima, H., Narumiya, S., and Numa, S. (1989) *Nature* **340,** 230–233.
18. Singer, D., Biel, M., Lotan, I., Flockerzi, V., Hofmann, F., and Dascal, N. (1991) *Science* **253,** 1553–1557.
19. Striessnig, J., Grabner, M., Nitterdorfer, J., Hering, S., Sinnergger, M. J., and Glossmann, H. (1998) *Trends Pharmacol. Sci.* **19,** 108–115.
20. Motoike, H. K., Bodi, I., Nakayama, H., Schwartz, A., and Varadi, V. (1999) *J. Biol. Chem.* **274,** 9409–9420.
21. Hofman F., Biel, M., and Flocherzi, V. (1994) *Annu. Rev. Neurosci.* **17,** 399–418.
22. Catterall, W. A., and Striessnig, J. (1992) *Trends Pharmacol. Sci.* **13,** 256–262.
23. Doyle, D. A., Morais Cabral, J., Pfuetzner, R. A., Kuo, A., Gulbis, J. M., Cohen, S. L., Chait, B. T., and MacKinnon, R. (1998) *Science* **280,** 69–77.
24. Chang, G., Spencer, R. H., Lee, A. T., Barclay, M. T., and Rees, D. C. (1998) *Science* **282,** 2220–2226.
25. Murata, K., Mitsuoka, K., Hirai, T., Walz, T., Agre, P., Heymann, J. B., Engel, A., and Fujiyoshi, Y. (2000) *Nature* **407,** 599–605.

26. Sato, C., Ueno, Y., Asai, K., Takahashi, K., Sato, M., Engel, A., and Fujiyoshi, Y. (2001) *Nature,* in press.
27. Mitchell, R. D., Palade, P., and Fleischer, S. (1983) *J. Cell Biol.* **96,** 1008–1016.
28. Kuniyasu, A., Oka, K., Ide-Yamada, T., Hatanaka, Y., Abe, T., Nakayama, H., and Kanaoka, Y. (1992) *J. Biochem.* **112,** 235–242.
29. Laemmli, U. K. (1970) *Nature* **227,** 680–685.
30. Frank, J., Radermacher, M., Penczek, P., Zhu, J., Li, Y., Ladjadj, M., and Leith, A. (1996) *J. Struct. Biol.* **116,** 190–199.
31. van Heel, M., and Frank, J. (1981) *Ultramicroscopy* **6,** 187–194.
32. van Heel, M., and Stoffler-Meilicke, M. (1985) *EMBO J.* **4,** 2389–2395.
33. Saxton, W. O., and Baumeister, W. (1982) *J. Microsc.* **127**(Pt 2), 127– 138.
34. Curtis, B. M., and Catterall, W. A. (1984) *Biochemistry* **23,** 2113–2118.
35. Sato, C., Sato, M., Iwasaki, A., Doi, T., and Engel, A. (1998) *J. Struct. Biol.* **121,** 314–325.
36. Chavis, P., Fagni, L., Lansman, J. B., and Bockeart, J. (1996) *Nature* **382,** 719–722.
37. Murray, B. E., and Ohlendieck, K. (1997) *Biochem. J.* **324**(Pt. 2), 689–696.
38. Fan, H., Brandt, N. R., Peng, M., Schwartz, A., and Caswell, A. H. (1995) *Biochemistry* **34,** 14893–14901.
39. Flockerzi, V., Oeken, H. J., and Hofmann, F. (1986) *Eur. J. Biochem.* **161,** 217–224.
40. Rohrkasten, A., Meyer, H. E., Nastainczyk, W., Sieber, M., and Hofmann, F. (1988) *J. Biol. Chem.* **263,** 15325–15329.
41. O'Callahan, C. M., and Hosey, M. M. (1988) *Biochemistry* **27,** 6071–6077.
42. Nishimura, S., Takeshima, H., Hofmann, F., Flockerzi, V., and Imoto, K. (1993) *FEBS Lett.* **324,** 283–286.
43. Neely, A., Wei, X., Olcese, R., Birnbaumer, L., and Stefani, E. (1993) *Science* **262,** 575–578.
44. Block, B. A., Imagawa, T., Campbell, K. P., and Franzini-Armstrong, C. (1988) *J. Cell Biol.* **107,** 2587–2600.